# Optimal Process Planning for Laser Forming of Doubly Curved Shapes

**Chao Liu**

**Y. Lawrence Yao**

Department of Mechanical Engineering,
Columbia University,
New York, NY 10027

**Vijay Srinivasan**

IBM Corporation,
White Plains, NY 10604

*There has been a considerable amount of work carried out on two-dimensional laser forming. In order to advance the process further for industrial applications, however, it is necessary to consider more general cases and especially their process planning aspect. This paper presents an optimal approach to laser scanning paths and heating condition determination for laser forming of doubly curved shapes. Important features of the approach include the strain field calculation based on principal curvature formulation and minimal strain optimization, and scanning paths and heating condition (laser power and scanning velocity) determination by combining analytical and practical constraints. The overall methodology is presented first, followed by more detailed descriptions of each step of the approach. Two distinctive types of doubly curved shape, pillow and saddle shapes are focused on and the effectiveness of the proposed approach is validated by forming experiments.* [DOI: 10.1115/1.1643077]

## 1 Introduction

Compared with conventional forming techniques, laser forming (LF) of sheet metal does not require hard tooling or external forces and hence, can increase process flexibility and reduce the cost of the forming process when low-to medium-volume production or prototyping is concerned. It therefore has potential applications in aerospace, shipbuilding and other industries. Significant progress has been made in analyzing and predicting LF processes of sheet metal. To apply the LF process to real world problems, however, the inverse problem needs to be addressed, that is, to design process parameters (laser scanning paths and heating condition in terms of laser power and scanning velocity) given a desired shape. For general three-dimensional shapes, determining laser scanning paths and heating condition is not obvious since their relationship to the shapes is complicated.

Ueda et al. [1] investigated the development of a computer-aid process planning system for plate bending by line heating. They computed the strains using large deformation elastic finite element method (FEM) and decomposed strains into in-plane and bending components. They then chose regions with large in-plane strains as heating zones and selected heating direction normal to the principal strain. Their work in line heating provides relevant information for the LF process design. However, their approach to heating path determination is not well explained. Furthermore, they did not deal with how to determine the heating condition.

Jang and Moon [2] developed an algorithm to determine heating lines for plate forming by line heating method. They first calculated the lines of curvature of a prescribed surface and evaluated the points of extreme principal curvature along the lines. They then classified and grouped them based on their principal directions and distances between. The heating lines are obtained by linear regressions on the grouped points. However, this method only used straight heating lines, which are inappropriate for more complicated shapes. Also, it did not address the heating condition determination.

Yu and Patrikalakis [3] presented algorithms for optimal development of a smooth continuous curved surface into a planar shape. The development process is modeled by in plane strain from the curved surface to its planar development. The distribution of the appropriate minimum strain field is obtained by solving a constrained nonlinear programming problem. The optimal developed planar shape is obtained by solving an unconstrained nonlinear programming problem, which is based on the strain distribution from previous step. The algorithms presented are illuminating; however, they do not provide an explicit method on how to determine laser paths nor on how to determine heating conditions.

Given the understanding that analytical or numerical solutions to the inverse problem may be less fruitful, heuristic approaches have been attempted. A genetic algorithm (GA) based approach, which is an adaptive heuristic search algorithm premised on the evolutionary ideas of natural selection and genetic, was proposed by Shimizu [4] as an optimization engine to solve the inverse problem of the LF process. In his study, a set of arbitrarily chosen heat process conditions for a dome shape was encoded into strings of binary bits, which evolve over generations following the natural selection scheme. One of the important process parameters, heating path positions, was assumed given. To apply GA, it is necessary to specify crossover rate and mutation rate but their selection suffers from lack of rigorous criteria.

Focusing on a class of shapes, Liu and Yao [5] proposed a response surface methodology based optimization method for LF process design. The propagation of error technique is built into the design process as an additional response to be optimized via desirability function and hence make the design robust. To the same end, Cheng and Yao [6] proposed a genetic algorithm in LF process design. This approach uses several analytical equations based on theoretical analysis and experiment/numerical training to predict the geometry change occurring in the straight-line LF. Both methods were successful for a class of shapes; however, they are not directly applicable to general 3D shapes.

This study presents an optimal process planning strategy to determine scanning paths and heating condition for laser forming of general doubly curved shapes. The overall methodology is presented first, followed by more step-by-step descriptions of the proposed strategy. Two distinctive types of doubly curved surfaces, pillow and saddle shape are studied and the overall methodology is validated by experiments.

## 2 Problem Description

Sheet metal concerned in forming including laser forming is mostly of the type of thin plates, that is, it has the ratio of $10 < w/h < 100$, where $h$ is plate thickness and $w$ is a typical planar dimension of a plate [7]. The locus of points that lie at equal

Contributed by the Manufacturing Engineering Division for publication in the JOURNAL OF MANUFACTURING SCIENCE AND ENGINEERING. Manuscript received May 2003. Associate Editor: A. J. Shih.

distances from two faces of a plate defines a middle surface. This paper is concerned with thin plates and therefore the analysis of strains can be reduced to the analysis of their middle surface only. This study is not limited to small deflections. When the deformation is small, the middle surface is neutral and otherwise there are strains on the middle surface.

An arbitrary surface is not characterized globally, but only at local points. That is only a local shape can be known and be determined by the derivatives of the surface vector. The nature of the local shape is classified into four cases according to the Gaussian curvature and coefficients of second fundamental form ($L$, $M$ and $N$) at the point (see Section 3 for more details). They are elliptic case, which has a positive Gaussian curvature, hyperbolic case, which has a negative Gaussian curvature, parabolic case, which has zero Gaussian curvature and $L^2+M^2+N^2\neq 0$, and planar case, which has zero Gaussian curvature and $L=M=N=0$.

In engineering applications, surfaces are often classified as singly and doubly curved surfaces. A singly curved surface has zero Gaussian curvature at all points, like the parabolic case, and therefore can be formed by bending strain only. A doubly curved surface has non-zero Gaussian curvature, like the elliptic case and the hyperbolic case, and generally requires both in-plane and bending strains to form. Surfaces of many engineering structures are commonly fabricated as doubly curved shapes to fulfill functional requirements such as hydrodynamic, aesthetic, or structural. For example, a large portion of the shell plates of ship hulls or airplane fuselages are doubly curved surfaces. This paper is concerned with doubly curved surfaces. For thin plates, in-plane strain is usually much larger than the bending strain and therefore only the former is considered in this paper.

Two distinctive doubly curved surfaces are chosen as desired shapes in this study. They are a pillow shape, which has positive Gaussian curvature over the entire surface, and a saddle type, which has negative Gaussian curvature over the entire surface. Both surfaces are given in the form of Bezier surface. Points on a Bezier surface are given by the following equation [8]

$$\mathbf{r}(u,v)=\sum_{i=0}^{m}\sum_{i=0}^{n}\mathbf{r}_{ij}B_{i,m}(u)B_{j,n}(v)\quad u,v\in[0,1] \tag{1}$$

where $\mathbf{r}_{ij}$ is the $ij^{\text{th}}$ control point, $B_{i,n}(u)=C(n,i)u^i(1-u)^{n-i}$, and $C(n,i)$ is the binomial coefficient $C(n,i)=n!/i!(n-1)!$.

For a bicubic Bezier patch, sixteen points are required to determine a surface patch, the point on the surface patch can be expressed in the matrix form [8],

$$\mathbf{r}(u,v)=[(1-u)^3\ \ 3u(1-u)^2\ \ 3u^2(1-u)\ u^3]\mathbf{Q}\begin{bmatrix}(1-v)^3\\3v(1-v)^2\\3v^2(1-v)\\v^3\end{bmatrix} \tag{2}$$

where $\mathbf{Q}$ is a 4 by 4 matrix containing the sixteen control points $\mathbf{r}_{ij}$. The control points for the pillow shape are:

(0,0,0), (0,1/3,0.025), (0,2/3,0.025), (0,1,0)
(1/3,0,3.0.042), (1/3,1/3,0.08), (1/3,2/3,0.08), (1/3,1,0.042)
(2/3,0,0.042), (2/3,1/3,0.08), (2/3,2/3,0.08), (2/3,1,0.042)
(1,0,0), (1,1/3,0.025), (1,2/3,0.025), (1,1,0)

For the saddle shape, the control points are:

(0,0,0.042), (0,1/3,0.017), (0,2/3,−0.017), (0,1,−0.042)
(1/3,0,3.0.017), (1/3,1/3,0.008), (1/3,2/3,−0.008), (1/3,1,−0.017)
(2/3,0,−0.017), (2/3,1/3,−0.008), (2/3,2/3,0.008), (2/3,1,0.017)
(1,0,−0.042), (1,1/3,−0.017), (1,2/3,0.017), (1,1,0.042)

These two shapes are shown in Figs. 1 and 2, respectively. As noticed in Fig. 1, the adjacent sides of the pillow shape are not identical, with the one along the $u$ direction curves slightly higher. The saddle shape in Fig. 2 bends up at a pair of opposite corners and down at the other pair.

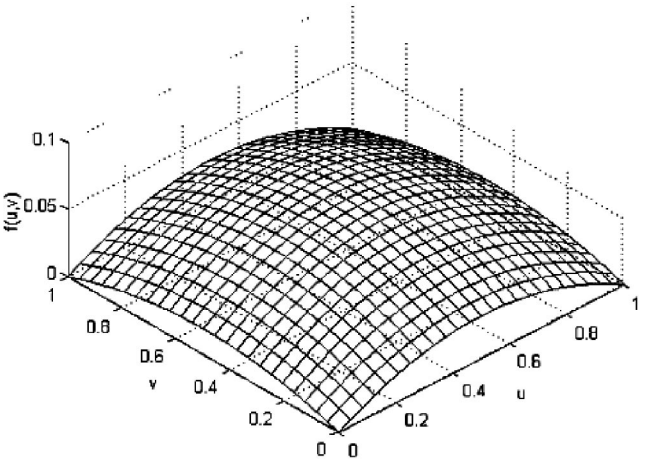


**Fig. 1 Desired pillow shape (also note the shape along the *u*-direction curves higher than that along the *v*-direction)**

Figure 3 outlines the overall strategy of process planning in this paper. The strategy consists of three stages. In stage one, the principal curvature directions are calculated based on the first and second fundamental form coefficients of a given doubly curved surface. Once the desired surface is given, the principal curvature directions can be determined. The desired doubly curved surface is then developed into a planar shape to obtain the required strain field. This part is modeled by in-plane strain along the principal curvature direction from the doubly curved surface to its planar development. The distribution of the minimum strain field is obtained by solving a constrained nonlinear optimization problem. Based on the strain field and the coefficients of the first fundamental form of the curved surface, the initial planar shape is obtained by solving an unconstrained nonlinear optimization problem.

In stage two, the planning of laser paths is carried out on the planar developed surface and perpendicular to the principal curvature directions solved from the stage one. Since the strains along the principal curvatures are perpendicular to each other, and no shear strain is considered, they can be regarded as the principal strains. Furthermore, it is well known that in a laser forming process, the largest compressive strains are generated perpendicular to the scanning path. Therefore, the laser path should be placed perpendicular to the principal curvature directions. Segmentation along the heating paths is performed and heating condition is de-

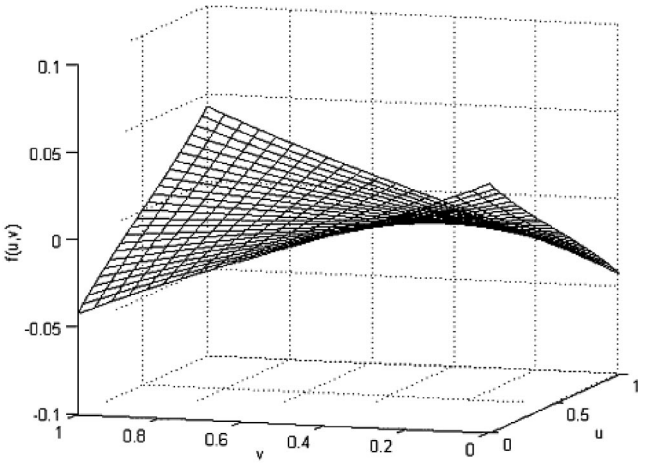


**Fig. 2 Desired saddle shape**

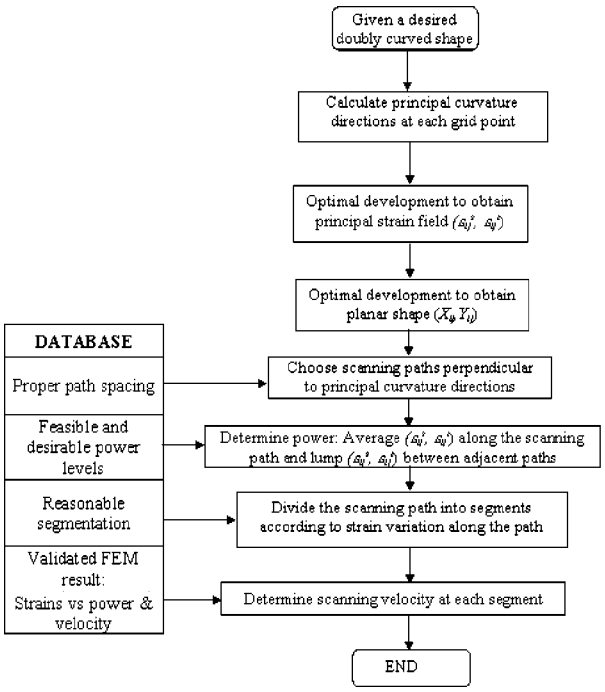


**Fig. 3 Outline of the process planning scheme**

termined in the final stage. The required strain between adjacent scanning paths is first lumped together, and a database, which is obtained from finite element method concerning the relationship between principal strains and laser power levels and scanning velocities, is then consulted. The three stages are described in more details in the following three sections.

## 3 Determination of Strain Field

In geometric modeling, shapes are commonly expressed in terms of parametric equations because the shapes of most objects are intrinsically independent of any coordinate system; the curves and surfaces are often nonplanar and bounded in some sense and cannot be represented by an ordinary nonparametric function; and a parametric representation is easier for the study on the local properties.

A parametric representation of a surface can be denoted by $\mathbf{r}=\mathbf{r}(u,v)$ where $(u,v)\in[0,1]$ forms a parametric space. Its partial derivatives at point $P$ on the surface are represented by $\mathbf{r}_u=\partial\mathbf{r}/\partial u$, $\mathbf{r}_v=\partial\mathbf{r}/\partial v$, $\mathbf{r}_{uu}=\partial^2\mathbf{r}/\partial u^2$, $\mathbf{r}_{vv}=\partial^2\mathbf{r}/\partial v^2$, and $\mathbf{r}_{uv}=\partial^2\mathbf{r}/\partial u\partial v$. A surface is uniquely determined by the first and second fundamental forms, which are local invariant quantities. The first fundamental form is a measure of the amount of movement of a surface at point $P$ in the parameter space and is defined as [9]

$$I=d\mathbf{r}\cdot d\mathbf{r}=Edu^2+2Fdudv+Gdv^2 \tag{3}$$

where

$$E=\mathbf{r}_u\cdot\mathbf{r}_u,\quad F=\mathbf{r}_u\cdot\mathbf{r}_v\quad\text{and}\quad G=\mathbf{r}_v\cdot\mathbf{r}_v \tag{4}$$

It's a homogeneous function of second degree in $du$ and $dv$ with coefficients $E$, $F$ and $G$. The second fundamental form measures the change in normal vector $d\mathbf{N}$ and the change of surface position $d\mathbf{r}$ at a surface point at $(u,v)$ as a function of a small movement $(du,dv)$ in the parameter space and is defined as.

$$II=-d\mathbf{r}\cdot d\mathbf{N}=Ldu^2+2Mdudv+Ndv^2 \tag{5}$$

where $L=-\mathbf{r}_u\cdot\mathbf{N}_u$, $M=(-1/2)(\mathbf{r}_u\cdot\mathbf{N}_v+\mathbf{r}_v\cdot\mathbf{N}_u)$, and $N=-\mathbf{r}_v\cdot\mathbf{N}_v$ are the second fundamental coefficients, and $\mathbf{N}_u=\partial\mathbf{N}/\partial u$ and $\mathbf{N}_v=\partial\mathbf{N}/\partial v$.

Let $\mathbf{r}=\mathbf{r}(u(s),v(s))$ be a curve $C$ on the surface through point $P$, where $s$ represents the arc length. $\mathbf{k}_n$ is the vector projection of the curvature vector $\mathbf{k}$ of the curve $C$ at point $P$ onto the normal $\mathbf{N}$ at $P$, i.e., $\mathbf{k}_n=(\mathbf{k}\cdot\mathbf{N})\mathbf{N}=\kappa_n\mathbf{N}$, where $\kappa_n$ is known as the normal curvature of the surface at $P$ and is expressed in terms of the first and second fundamental form, namely,

$$\kappa_n=\frac{Ldu^2+2Mdudv+Ndv^2}{Edu^2+2Fdudv+Gdv^2}=\frac{II}{I} \tag{6}$$

**3.1 Principal Curvatures.** Principal directions are the two perpendicular directions at which the value $\kappa_n$ take on maximum and minimum values, and the corresponding normal curvatures, $\kappa_{\min}$ and $\kappa_{\max}$, are the principal curvatures. The value of principal curvatures and principal directions at a point $P$ on a surface can be obtained by taking derivative of Eq. (6) with respect to $\lambda=dv/du$ and letting it equal to zero, that is,

$$(FN-MG)\lambda^2+(EN-LG)\lambda+(EM-LF)=0 \tag{7}$$

where $\lambda$ is a principal direction at $P$. Substituting $\lambda$ into Eq. (6) yields

$$(EG-F^2)\kappa_n^2-(EN+GL-2FM)\kappa_n+(LN-M^2)=0 \tag{8}$$

Gaussian curvature is the product of the roots of Eq. (8), $\kappa_{\min}$ and $\kappa_{\max}$ that is

$$K=\kappa_{\min}\kappa_{\max}=\frac{LN-M^2}{EG-F^2} \tag{9}$$

The Gaussian curvature $K$ can also be expressed in terms of $E$, $F$, and $G$ and their derivatives (Eq. ($A1$) in Appendix). For a doubly curved surface, the Gaussian curvature is not equal to zero at least at some points on the surface, while a singly curved surface or planar surface, the Gaussian curvature is zero everywhere on the surface. A curve on a surface whose tangent at each point is along a principal direction is called a line of curvature. It follows that a curve is a line of curvature if and only if at each point the direction of its tangent satisfies Eq. (7) for some path $\mathbf{r}=\mathbf{r}(u,v)$.

**3.2 Strain Field for Planar Development.** Assume the strain field due to changing from a given curved surface to its planar shape is represented by $\varepsilon^s(u,v)$ and $\varepsilon^t(u,v)$ where $(s,t)$ denote the principal curvature directions. Knowing that the strain field can be expressed by the intrinsic geometric properties of the surfaces and that flattening a curved surface can yield multiple solutions of $\varepsilon^s(u,v)$ and $\varepsilon^t(u,v)$, an optimization approach is appropriate to solve the problem. An approach based on minimization of the total strain energy after adding the strain field to the given doubly curved surface, which maps to a planar shape on which Gaussian curvature $K_{ps}$ is zero everywhere [4], is expressed as

$$\begin{aligned}\min&\int\int_D\{(\varepsilon^s)^2+(\varepsilon^t)^2\}|\mathbf{r}_u\times\mathbf{r}_v|dudv\\&=\min\int\int_D\{(\varepsilon^s)^2+(\varepsilon^t)^2\}\sqrt{EG-F^2}dudv\end{aligned} \tag{10}$$

subject to $K_{ps}=0$, $\varepsilon^s(u,v)\geqslant 0$ and $\varepsilon^t(u,v)\geqslant 0$. $(u,v)\in D$ and $D$ is the parametric space.

In the above objective function, $\sqrt{EG-F^2}dudv$ is the area of a small region bounded by $du$ and $dv$. The physical meaning of the objective function therefore is to minimize the total strain energy along the principal curvature directions over the entire surface area. For the constraint $K_{ps}=0$, Eq. ($A1$) will be used by replacing $e$, $f$, and $g$ for $E$, $F$, and $G$, where $e$, $f$, and $g$ are the first fundamental form coefficients of the developed planar surface $\mathbf{R}(u,v)$ (Fig. 4) and defined as

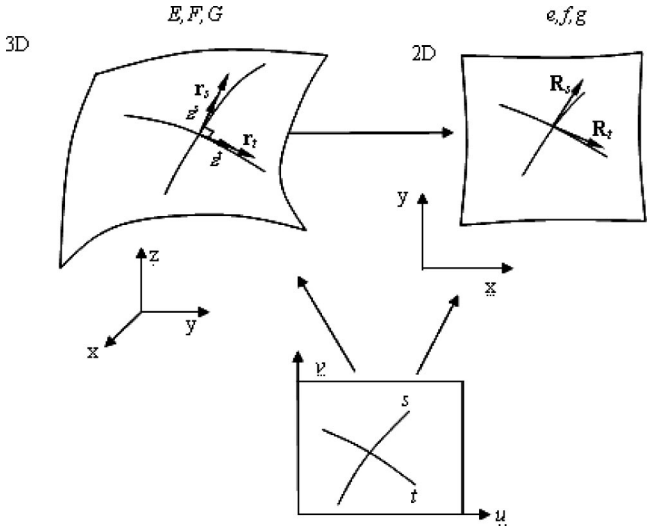


**Fig. 4 Doubly curved surface, its planar development and the strain definition**

$$e=\mathbf{R}_u\cdot\mathbf{R}_u,\quad f=\mathbf{R}_u\cdot\mathbf{R}_v,\quad \text{and}\quad g=\mathbf{R}_v\cdot\mathbf{R}_v \tag{11}$$

It is more convenient to use the form shown in Eq. (*A*1) than in Eq. (9) because only the first fundamental form coefficients and their derivatives are needed. The relationships between *e*, *f*, and *g* and the given curved surface parameters as well as the unknowns $\varepsilon^s(u,v)$ and $\varepsilon^t(u,v)$ are briefly derived in Eq. (*A*2) to (*A*6).

The non-negativity constraints $\varepsilon^s(u,v)\geqslant 0$ and $\varepsilon^t(u,v)\geqslant 0$ are imposed for the following reason. During a laser forming process, it is known that the strains generated to form a planar shape to a curved surface are mostly compressive, that is, $e^s(u,v)\leqslant 0$, and $e^t(u,v)\leqslant 0$. As a result, the strains required to develop the curved surface to its planar shape are tensile, that is, $\varepsilon^s(u,v)\geqslant 0$ and $\varepsilon^t(u,v)\geqslant 0$.

Equation (10), representing a constrained nonlinear optimization problem, is discretized by using the trapezoidal rule of integration and central difference method for partial derivatives in the constraints (Eq. (*A*7)). If the space *D* is discretized into *m* by *n* grid points, there are $2mn$ decision variables $\varepsilon^s_{ij}$ and $\varepsilon^t_{ij}$, $i=1,2,\ldots,m$, and $j=1,2,\ldots,n$. NAG e04ucf routine [10], which implements a sequential quadratic programming method (SQP) is used to solve the constrained nonlinear optimization problem. The results are shown in Figs. 5 and 6 for the pillow and saddle cases, respectively. The length of the bars represents the magnitude and the orientation of the bars the direction of the strains.

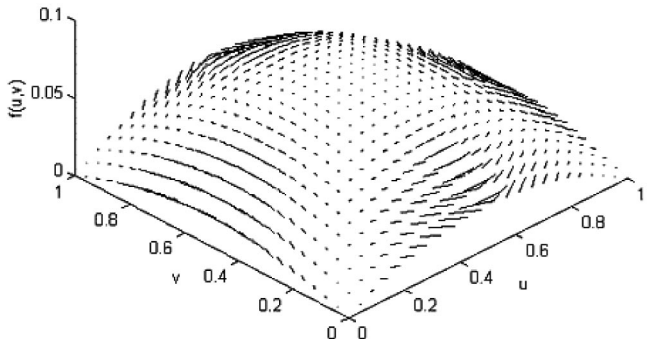


**Fig. 5 Strains along principal curvature directions on the pillow shape (the segment length represents the strain magnitude and the segment orientation represents the strain direction)**

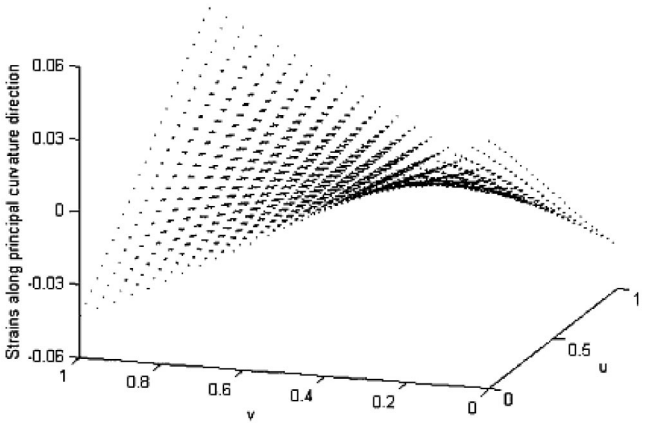


**Fig. 6 Strains along principal curvature directions on the saddle shape (the segment length represents the strain magnitude and the segment orientation represents the strain direction)**

**3.3 Planar Developed Shape.** After obtaining the strain field ($\varepsilon^s_{ij}$ and $\varepsilon^t_{ij}$) at all grid points, the planar coordinates $(X_{ij},Y_{ij})$ of the grid points corresponding to the planar developed shape can be determined. This will give the size and profile of the planar developed shape, which are needed in cutting the planar shape to form the desired curved surface.

The decision variables to be determined are the $2mn$ coordinates of the grid points $\mathbf{R}_{ij}=(X_{ij},Y_{ij})$, which are supposed to satisfy Eq. (11), where *e*, *f* and *g* are determined based on ($\varepsilon^s_{ij}$ and $\varepsilon^t_{ij}$) and other information of the desired curved surface (Eq. (*A*6)). As a result, Eq. (11) gives $3mn$ known conditions. To solve this over-determined system of nonlinear polynomial equations, the following unconstrained least square error minimization problem is solved by using quasi-Newton method in NAG C routine e04fcc.

$$\min\sum_{i=1}^{m}\sum_{j=1}^{n}(\mathbf{R}_u\cdot\mathbf{R}_u|_{ij}-e_{ij})^2+(\mathbf{R}_u\cdot\mathbf{R}_v|_{ij}-f_{ij})^2+(\mathbf{R}_v\cdot\mathbf{R}_v|_{ij}-g_{ij})^2 \tag{12}$$

where $\mathbf{R}_u$ and $\mathbf{R}_v$ are expressed in terms of $(X_{ij},Y_{ij})$ using the finite difference method. The initial points of the minimization problem are given by $(X_{ij},Y_{ij})=(i/m,j/n)$ where $i=1,\ldots,m$; $j=1,\ldots,n$. The results are shown in Figs. 7 and 8 for the pillow and saddle cases, respectively.

**3.4 Curved Surface Reconstruction.** To validate the strain field and planar shape development process, the coordinates of the given curved surface $\mathbf{r}_{ij}=(x_{ij},y_{ij},z_{ij})$ can be reconstructed by solving the following least squares error minimization problem [4]:

$$\begin{aligned}\min\sum_{i=1}^{m}\sum_{j=1}^{n}&(\mathbf{r}_u\cdot\mathbf{r}_u|_{ij}-E_{ij})^2+(\mathbf{r}_u\cdot\mathbf{r}_v|_{ij}-F_{ij})^2+(\mathbf{r}_v\cdot\mathbf{r}_v|_{ij}-G_{ij})^2\\&+(\mathbf{r}_{uu}\cdot(\mathbf{r}_u\times\mathbf{r}_v)|_{ij}-L_{ij}\sqrt{E_{ij}G_{ij}-F_{ij}^2})^2+(\mathbf{r}_{uv}\cdot(\mathbf{r}_u\times\mathbf{r}_v)|_{ij}\\&-M_{ij}\sqrt{E_{ij}G_{ij}-F_{ij}^2})^2+(\mathbf{r}_{vv}\cdot(\mathbf{r}_u\times\mathbf{r}_v)|_{ij}-N_{ij}\sqrt{E_{ij}G_{ij}-F_{ij}^2})^2\end{aligned} \tag{13}$$

where $E_{ij}$, $F_{ii}$, and $G_{ij}$ are calculated based on the $e_{ij}$, $f_{ij}$, and $g_{ij}$ and the strain field ($\varepsilon^s_{ij}$ and $\varepsilon^t_{ij}$) using a discrete version of Eq. (*A*6), and $e_{ij}$, $f_{ij}$, and $g_{ij}$ are computed based on the planar coordinates $(X_{ij},Y_{ij})$ using a discrete version of Eq. (11). The results are shown in Figs. 9 and 10 for the pillow and saddle

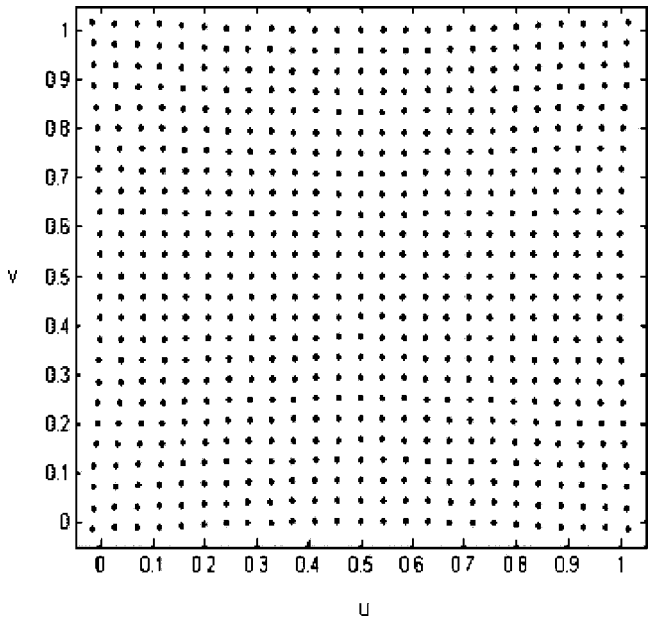


**Fig. 7 Planar developed shape of the pillow case (distortion from the original parametric space $D:(u,v)\in[0,1]$ is magnified by a factor of 5 for viewing clarity)**

cases, respectively. As seen, the reconstructed curved surfaces agree with the given ones and the process of strain field and planar developed surface determination is validated.

**3.5 Strain Field Transformation.** The strains $\varepsilon^s(u,v)$ and $\varepsilon^t(u,v)$ are on the curved surface and to determine scanning paths on the planar developed surface, they need to be transformed onto the planar surface $e^s(u,v)$ and $e^t(u,v)$. Since $\varepsilon^s(u,v)$ and $\varepsilon^t(u,v)$ represent the strains due to changing from curved surface to its planar development, an infinitesimal length $|\mathbf{r}_s ds|$ changes to $(1+\varepsilon^s)|\mathbf{r}_s ds|$ and $|\mathbf{r}_t dt|$ changes to $(1+\varepsilon^t)|\mathbf{r}_t dt|$ (Fig. 4). Therefore,

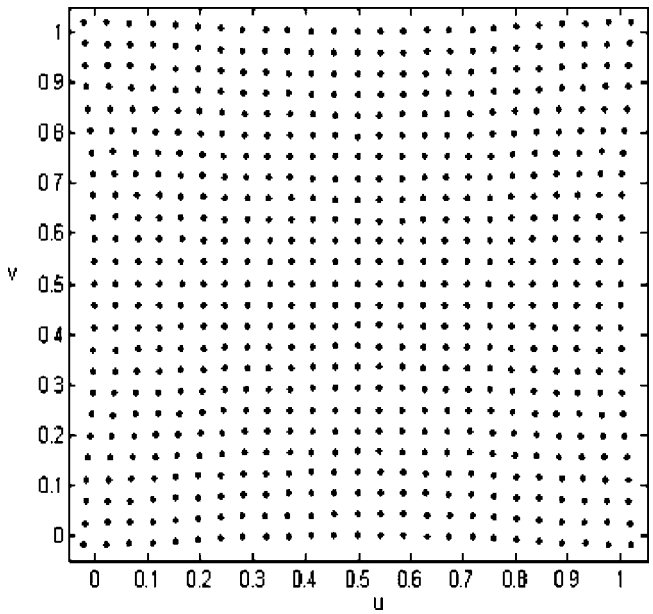


**Fig. 8 Planar developed shape of the saddle case (distortion from the original parametric space $D:(u,v)\in[0,1]$ is magnified by a factor of 5 for viewing clarity)**

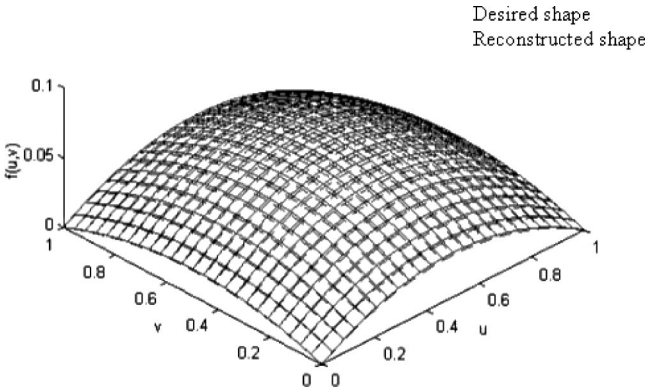


**Fig. 9 Comparison between desired and reconstructed shapes of the pillow case (the difference between the two surfaces is multiplied by 5 for viewing clarity)**

$$|\mathbf{R}_s|=(1+\varepsilon^s)|\mathbf{r}_s|, \quad \text{and} \quad |\mathbf{R}_t|=(1+\varepsilon^t)|\mathbf{r}_t|, \tag{14}$$

where $\mathbf{r}$ and $\mathbf{R}$ represent the given curved surface and its planar development, respectively and $(s,t)$ represent the principal curvature directions. Similarly,

$$|\mathbf{r}_s|=(1+e^s)|\mathbf{R}_s|, \quad \text{and} \quad |\mathbf{r}_t|=(1+e^t)|\mathbf{R}_t|, \tag{15}$$

Combining Eqs. (14) and (15), $e^s(u,v)$ and $e^t(u,v)$ can be expressed in terms of $\varepsilon^s(u,v)$ and $\varepsilon^t(u,v)$ as

$$e^s=-\frac{\varepsilon^s}{1+\varepsilon^s}, \quad \text{and} \quad e^t=-\frac{\varepsilon^t}{1+\varepsilon^t} \tag{16}$$

As seen in Eq. (16) and discussed in Section 3.2, $e^s(u,v)$ and $e^t(u,v)$ have opposite signs as $\varepsilon^s(u,v)$ and $\varepsilon^t(u,v)$. The results are shown in Figs. 11 and 12 for the pillow and saddle cases, respectively.

## 4 Scanning Paths

After a strain field required to develop a desired curved shape to its planar shape is determined, scanning paths are designed. It is well known that, in the laser forming process, the highest compressive strains occur in a direction perpendicular to a scanning path and in-plane within workpiece. Therefore a scanning path should be perpendicular to the direction of the principal strain. Since the strains developed along the principal curvature directions $(\varepsilon^s,\varepsilon^t)$ in the preceding section are perpendicular to each other and no shear strain is involved in the process, they can be

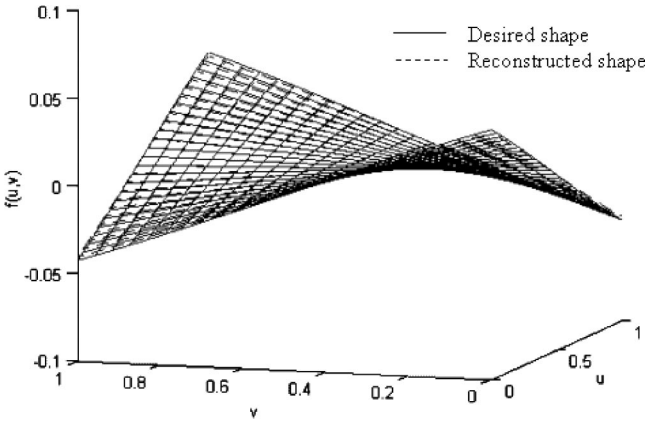


**Fig. 10 Comparison between desired and reconstructed shapes of the saddle case (the difference between the two surfaces is multiplied by 5 for viewing clarity)**

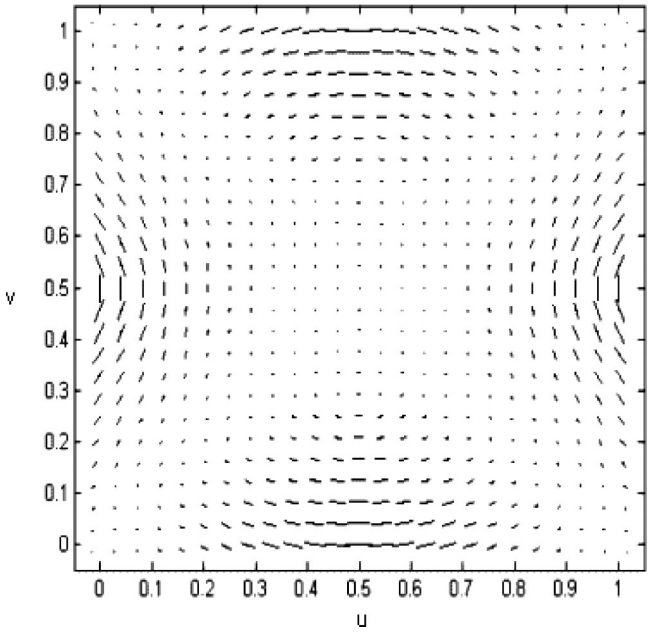


**Fig. 11 Strains along the principal curvature directions on the planar developed shape of the pillow case (the segment length represents the strain magnitude and the segment orientation represents the strain direction)**

regarded as the in-plane principal strains, and therefore a scanning path should be perpendicular to the direction of the principal curvature at every point on the path. In other words, a scanning path is the same as a line of curvature, that is, a curve on a surface whose tangent at each point is along a principal curvature direction of the surface.

For the laser forming based on the temperature gradient mechanism [11], the target bends towards the heating source and the

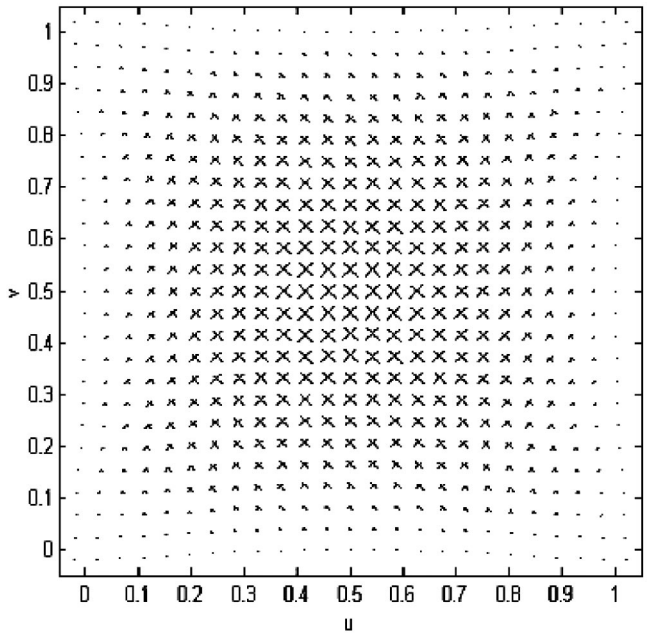


**Fig. 12 Strains along the principal curvature directions on the planar developed shape of the saddle case (the segment length represents the strain magnitude and the segment orientation represents the strain direction)**

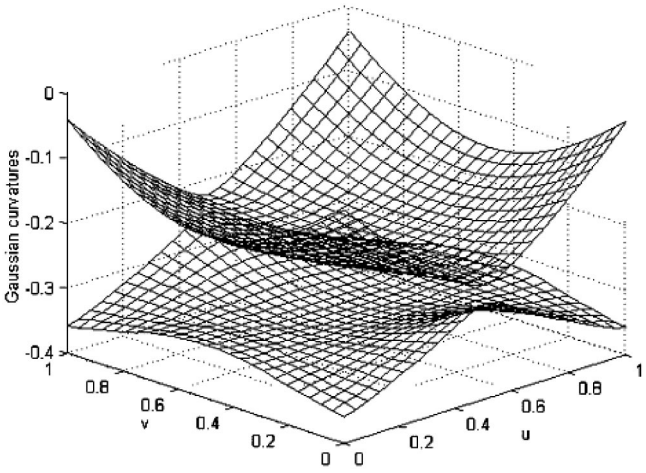


**Fig. 13 Magnitude of principal curvatures of the pillow shape showing that all the principal curvatures have negative values**

curvature generated is considered positive. To form a curved surface by laser forming is to superpose these positive curvatures on the appropriate regions of the plate. If the Gaussian curvatures along the lines of curvature are positive, the scanning paths should be placed on one side of the plate. If the Gaussian curvatures are negative, the scanning paths should be placed at both sides of the plate. Figure 13 shows that the principal curvatures are both negative in the pillow shape, namely Gaussian curvatures are positive all over the plate. As a result, all the laser paths should be positioned on one side of the plate. Fig. 14, however, shows a different scenario. For the saddle shape, each location on the plate has both positive and negative principal curvatures. Therefore, the laser paths should be positioned at both sides of the plate.

In determining the spacing of adjacent scanning paths, the following guidelines are followed and the guidelines are included in the database shown in Fig. 1. In general, the smaller the spacing, the more precise the desired shape can be formed. However, the adjacent paths cannot be too close since they will no longer be independent with each other while independence is a requirement assumed in determining the heating condition in the next section. Fig. 15 shows that temperature and compressive plastic strain rise do not go beyond the extent of laser beam size in laser forming and therefore the minimal spacing equals the laser beam radius. In addition, too small spacing implies more scanning and thus longer

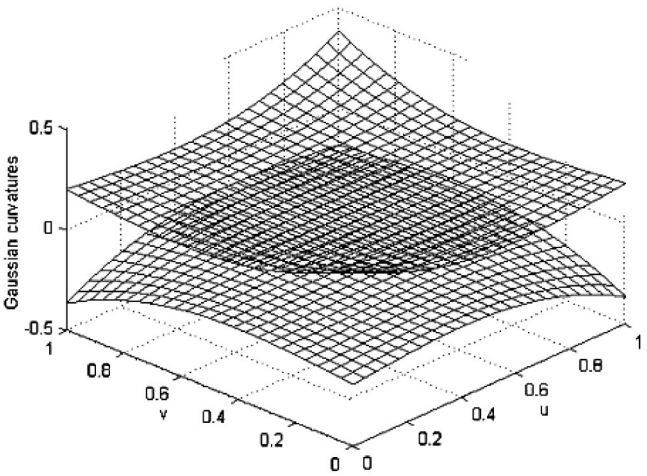


**Fig. 14 Magnitude of principal curvatures of the saddle shape showing that they have both positive and negative values**

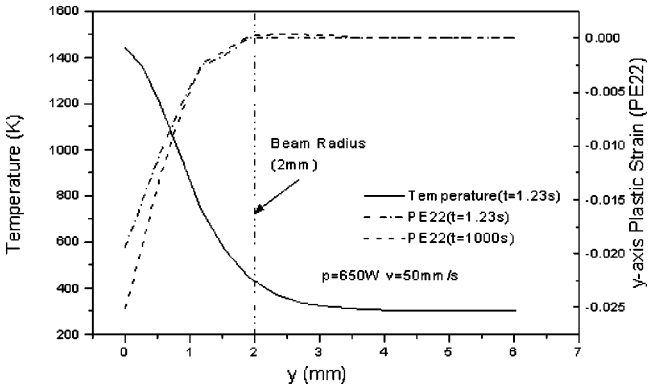


**Fig. 15 Typical simulation results showing temperature and compressive plastic strain rise do not go beyond the extent of laser beam size (beam diameter is 4 mm, scanning path at $y = 0$ mm, square 1010 steel plate of 80 by 80 by 0.89 mm) [5]**

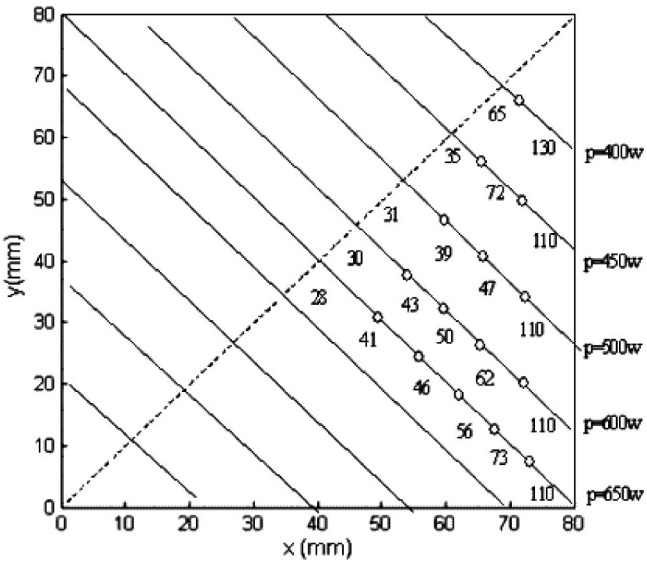


**Fig. 17 Optimal planning of laser paths (shown in lines) and heating condition (power shown in watts and scanning speed shown in numbers with unit of mm/s) for the saddle shape. Only a quarter of the paths/condition is shown due to symmetry. Material is 1010 steel. Beam spot size is 6 mm. The dotted line represents a scanning path on the opposite side of the plate and other paths on the opposite side (similar to the ones on the side shown) are not shown for viewing clarity.**

time to form a part. The strain distribution over the entire plate should also be considered in determining the spacing of adjacent paths. The regions of a shape that has larger strains need to be scanned with denser paths. As a rule of thumb, spacing between two adjacent paths, $D_{paths}$, should be equal to strain generated by laser forming, $\varepsilon_{laser}$, multiplied by laser beam spot size, $d_{laser}$ and divided by the average principal strain over the spacing. Another consideration is where to not place a scanning path or where to terminate a scanning path. If a region has strains smaller than a particular value of the maximum strain in the plate, say 5%, no scanning paths are placed there. Similarly, if the strain along a scanning is smaller than a particular value, the scanning path is terminated at that point.

Figures 16 and 17 show the scanning paths determined using the above principles and guidelines in order to form the pillow shape and saddle shape, respectively. The power and scanning speed shown will be explained in the next section. As seen from Fig. 16 (only a quarter of the plate is shown due to symmetry), the scanning paths are perpendicular to the principal curvature directions. This is also the case for Fig. 17 where the directions (shown in Fig. 12) are not shown for viewing clarity. In the pillow case the regions around the mid edges have larger strains, while regions at the corners and the center of the plate have smaller strains. Based on previous discussions, the laser paths should be positioned denser around the mid edges of the plate. On the other hand, in the saddle shape (only a quarter of paths are shown due to symmetry), the strains are larger at the center of the plate and become smaller towards the edges (Fig. 12). Therefore, laser paths should be denser at the center of the plate. Regions with strains less than 5% of the maximal strain of the plate, no paths are placed. A laser path terminates where the corresponding strain is less than 5% of the maximum strain along the path. As seen, the determination of the scanning paths involves certain practical considerations which are included in the database shown in Fig. 1 and the solution is obviously not unique.

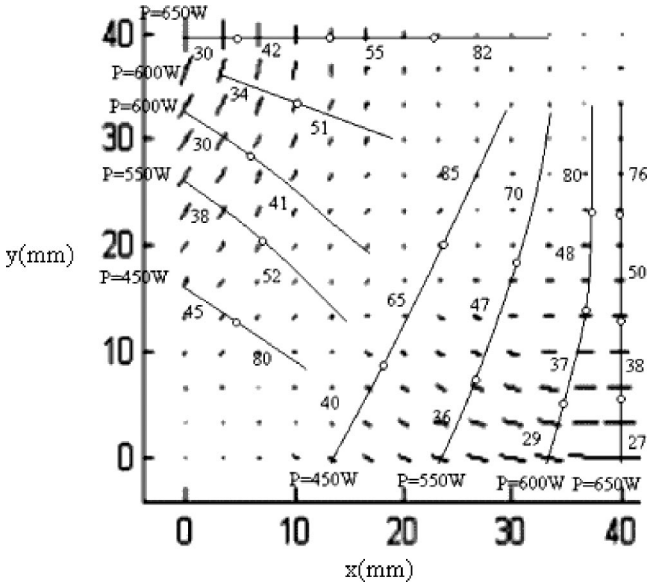


**Fig. 16 Optimal planning of laser paths (shown in line segments) and heating condition (power shown in watts and scanning speed shown in numbers with unit of mm/s) for the pillow shape. A quarter of a 80 by 80 by 0.89 mm plate is shown due to symmetry. Material is 1010 steel. Beam spot size is 6 mm. Shown in background are strains.**

## 5 Heating Condition

The final stage of 3D laser forming design is to determine the heating condition. If the plate dimension and the laser spot size are given, the heating condition that needs to be determined includes laser power and laser scanning velocity. In this study, the selected samples are 1010 steel coupons with dimension of 80 by 80 by 0.89 mm. Figure 18 shows principal minimum strain averaged over a beam spot size as a function of laser power and scanning velocities determined via finite element analysis of single straight-line (independent) laser scanning of a plate with the above material and dimension. Detailed FEM modeling description can be found in Liu and Yao [5]. This relationship is part of the database shown in Fig. 3. As seen, there are many possible combinations of power and velocity to realize a given strain. The strategy to determine the heating condition is summarized below.

First, the in-plane strains along a scanning path determined in the section 4 are averaged and checked with Fig. 18 and a laser power level is chosen. This step is to ensure that the power level chosen is readily available in the existing laser forming equipment. The laser power is kept constant for the laser path. The next

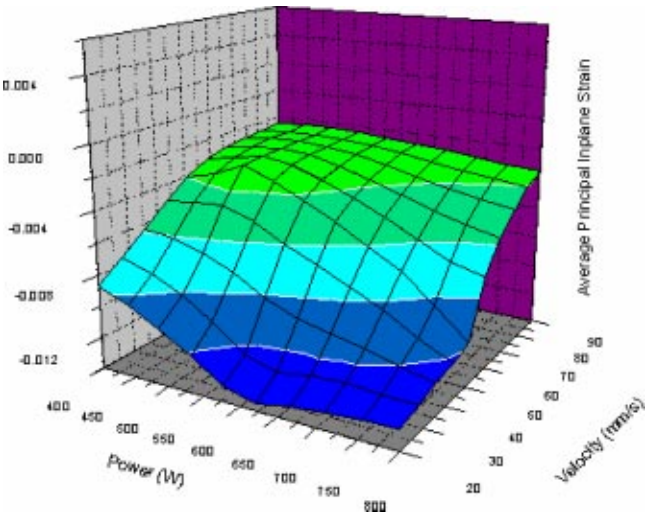


**Fig. 18 Average principal in-plane strain vs. power and velocity from FEM analysis. The average is carried out over the laser beam radius (beam diameter is 4 mm, square 1010 steel plate of 80 by 80 by 0.89 mm) [6].**

step is to determine the velocities along the path. In general, the strain distribution along the path is not uniformly distributed; therefore the velocity ideally should vary with the strain along the path. Practically, a laser path is broken into several segments so that in each segment the strain variation is not larger than, say, 1/5 of the maximum strain along the path. A constant velocity is prescribed for each segment based on the average strain of the segment, predetermined laser power, and the existing relationship shown in Fig. 18. The average strain of the segment is obtained by averaging the strain along the segment, followed by lumping the strain between adjacent paths.

The heating condition for the two desired shapes is decided following the above strategy and superposed in Figs. 16 and 17, respectively. Generally, regions requiring high strains get higher power levels and lower velocities prescribed simply because more energy input is required. For example for the path at $x=40$ mm in Fig. 16, where the highest strain is required, the power is highest at 650 W for the path. At locations near $y=0$ on the path, the strains are larger, therefore the velocity is lowest ($v=27$ mm/s). As the path moves toward the center, the velocity increases sharply, due to the quick drop of strain. Since the strain gradient along the path slows down towards the center of the plate, the segment spacing becomes larger accordingly. On the contrary, the principal strains are larger at the center of the plate for the saddle case shown in Fig. 17, and therefore the spacing of the adjacent paths are denser. But the strain gradients are larger towards edges and corners of the plate, the segment spacing is therefore smaller towards the edges and corners.

## 6 Experimental Validation

Laser forming experiments were conducted on 1010 steel coupons of dimension of 80 by 80 by 0.89 mm, the same as used in simulation. The scanning paths and heating condition in the experiments are shown in Figs. 16 and 17 for the pillow and saddle cases, respectively. The laser system used is a PRC-1500 $CO_2$ laser, which has a maximum output power of 1,500 W. Laser beam spot size used is 4 mm. Workpiece movement was controlled by Unidex MMI500 motion control system, which allows convenient specifications of variable velocities along a path with smooth transitions from segment to segment.

Figure 19 shows the formed pillow and saddle shape under these conditions. A coordinate measuring machine (CMM) is used to measure the geometry of the formed shapes. Figures 20 and 21 compare the geometry of formed shape under the determined conditions and desired shape. Only the geometry of top surface of the plate is measured and a general agreement can be seen from the figures. There is about 10% error for the saddle case especially at the corners seen from Fig. 21. Possible sources of error include the average and lumped method used to determine strains of path segments, and the approximate method used to determine the laser power and scanning velocity based on independent scans. After all, a strain field required to develop a curved shape to its planar shape is continuous in nature while the laser forming process uses a discrete number of paths to approximate the strain field.

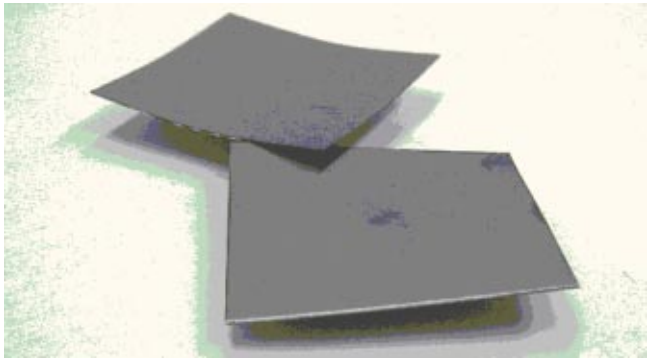

**Fig. 19 Laser formed pillow and saddle shapes using the process plans shown in Figs. 15 and 16, respectively (1010 steel plate of 80 by 80 by 0.89 nm, beam diameter is 4 mm)**

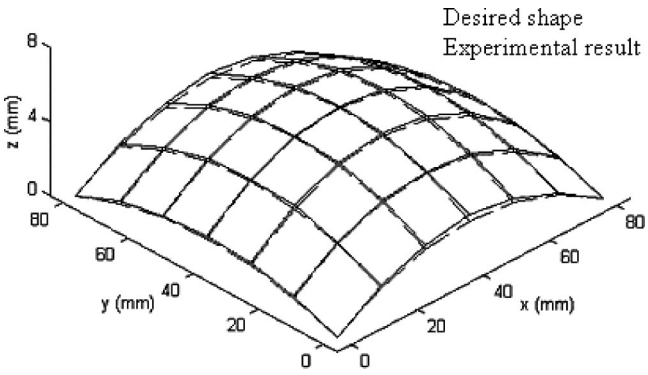


**Fig. 20 Comparison of desired and measured shapes of the pillow case (an array of 7 by 7 points measured by CMM)**

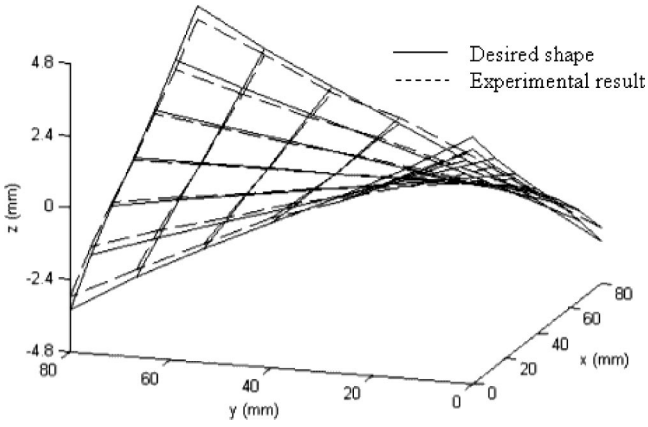


**Fig. 21 Comparison of desired and measured shapes of the saddle case (an array of 7 by 7 points measured by CMM)**

## 7 Conclusions

Reconstruction of the desired doubly curved shapes shows the strain field determination based on principal curvature formulation and minimal strain optimization is effective and of sufficient precision. The concept of determining a strain field required to develop a given curved shape to its planar shape as the first step of process planning for laser forming is of merit. Placing scanning paths perpendicular to the principal curvature directions, namely along the line of curvatures of a desired shape proves to be unambiguous and easy to implement. Practical constraints need to be combined with analytical ones in determining path spacing and heating condition. There is a trade-off between forming accuracy and efficiency by carefully choosing density of scanning paths and path segments.


## Acknowledgment

Support from NSF under grant DMI-0000081 is gratefully acknowledged. Valuable discussions with Prof. T. Maekawa of MIT are also appreciated.


## Appendix

Equation (9) shows Gaussian curvature $K$ is expressed in terms of the first and second fundamental form coefficients of a surface. In practice, $K$ can be alternatively expressed as a function of the first fundamental form coefficients and their derivatives [12].

$$K=\{E(E_vG_v-2F_uG_v+G_u^2)+F(E_uG_v-E_vG_u-2E_vF_v+4E_uF_v-2F_uG_u)+G(E_uG_u-2E_uF_v+E_v^2)-2(EG-F^2)(E_{vv}-2F_{uv}+G_{uu})\}/4(EG-F^2)^2 \quad (A1)$$

From the definition of first fundamental form coefficients (Eqs. (4) and (11),

$$\mathbf{R}_s\cdot\mathbf{R}_s=(\mathbf{R}_uu_s+\mathbf{R}_vv_s)\cdot(\mathbf{R}_uu_s+\mathbf{R}_vv_s)=eu_s^2+2\,fu_sv_s+gv_s^2$$
$$\mathbf{r}_s\cdot\mathbf{r}_s=(\mathbf{r}_uu_s+\mathbf{r}_vv_s)\cdot(\mathbf{r}_uu_s+\mathbf{r}_vv_s)=Eu_s^2+2Fu_sv_s+Gv_s^2 \quad (A2)$$

Using Eqs. (*A*1), (*A*2), and (14), one obtains

$$eu_s^2+2\,fu_sv_s+gv_s^2=(1+\varepsilon^s)^2(Eu_s^2+2Fu_sv_s+Gv_s^2). \quad (A3)$$

Similarly, along the minimal principal curvature direction, one obtains

$$eu_t^2+2\,fu_tv_t+gv_t^2=(1+\varepsilon^t)^2(Eu_t^2+2Fu_tv_t+Gv_t^2) \quad (A4)$$

Assume the principal curvature directions remain orthogonal after development, which implies

$$\mathbf{R}_s\cdot\mathbf{R}_t=(\mathbf{R}_uu_s+\mathbf{R}_vv_s)\cdot(\mathbf{R}_uu_t+\mathbf{R}_vv_t)=eu_su_t+f(u_sv_t+u_tv_s)+gv_sv_t=0 \quad (A5)$$

Equations (*A*3) to (*A*5) represent a system of three linear equations in $e$, $f$, and $g$, which are solved as

$$e=\frac{v_t^2[Eu_s^2+2Fu_sv_s+Gv_s^2](1+\varepsilon^s)^2+v_s^2[Eu_t^2+2Fu_tv_t+Gv_t^2](1+\varepsilon^t)^2}{(v_su_t-u_sv_t)^2}$$
$$f=-\frac{u_tv_t[Eu_s^2+2Fu_sv_s+Gv_s^2](1+\varepsilon^s)^2+u_sv_s[Eu_t^2+2Fu_tv_t+Gv_t^2](1+\varepsilon^t)^2}{(v_su_t-u_sv_t)^2} \quad (A6)$$
$$g=\frac{u_t^2[Eu_s^2+2Fu_sv_s+Gv_s^2](1+\varepsilon^s)^2+u_s^2[Eu_t^2+2Fu_tv_t+Gv_t^2](1+\varepsilon^t)^2}{(v_su_t-u_sv_t)^2}$$

For a given curved surface, $E$, $F$, and $G$ as well as $u_s$, $u_t$, $v_s$, and $v_t$ can be calculated, and therefore if $\varepsilon^s$ and $\varepsilon^t$ are calculated, $e$, $f$ and $g$ can be calculated accordingly.

The objective function of Eq. (10) can be discretized using the trapezoidal rule of integration and central difference method for partial derivatives [13]. After discretization, the objective function becomes

$$\sum_{i=1}^{m}\sum_{j=1}^{n}\alpha_{ij}((\varepsilon_{ij}^s)^2+(\varepsilon_{ij}^t)^2)\sqrt{E_{ij}G_{ij}-F_{ij}^2}\Delta u\Delta v \quad (A7)$$

$$\text{where}\begin{cases}\alpha_{ij}=1 & 1<i<m;1<j<n\\ \alpha_{ij}=0.5 & 1<i<m;j=1 \text{ or } j=n\\ \alpha_{ij}=0.5 & i=1 \text{ or } i=m;1<j<n\\ \alpha_{ij}=0.25 & i=j=1 \text{ or } i=m,j=n\\ \alpha_{ij}=0.25 & i=m;j=1;\text{or } i=1,j=n\end{cases}$$

$\Delta u$ and $\Delta v$ are the length between two adjacent grid points.

## References


[1] Ueda, K., Murakawa, H., Rashwan, A. M., Okumoto, Y., and Kamichika, R., 1994, ''Development of Computer-aided Process Planning System for Plate Bending by Line Heating (Report 1)-Relation Between Final Form of Plate and Inherent Strain,'' J. Ship Prod., **10(1)**, pp. 59–67.

[2] Jang, C. D., and Moon, S. C., 1998, ''An Algorithm to Determine Heating Lines for Plate Forming by Line Heating Method,'' J. Ship Prod., **14(4)**, pp. 238–245.

[3] Shimizu, H., 1997, ''A Heating Process Algorithm for Metal Forming by a Moving Heat Source,'' M.S. thesis, M.I.T.

[4] Yu, G., Patrikalakis, N. M., and Maekawa, T., 2000, ''Optimal Development of Doubly Curved Surfaces,'' Computer Aided Geometric Design, **17**, pp. 545–577.

[5] Liu, C., and Yao, Y. L., 2002, ''Optimal and Robust Design of Laser Forming Process,'' Trans. NAMRC XXX, 2002, pp. 39–46.

[6] Cheng, J., and Yao, Y. L., 2001, ''Process Synthesis of Laser Forming by Genetic Algorithms,'' *Proceedings of ICALEO 2001*, Section D 604.

[7] Ventsel, E., and Krauthammer, T., 2001, *Thin Plates and Shells*, Marcel Dekker Publishing Company, New York.

[8] Mortenson, M., 1985, *Geometric Modeling*, John Wiley & Sons, New York.

[9] Lipschultz, M., 1969, *Theory and Problems of Differential Geometry*, McGraw-Hill.

[10] Numerical Algorithms Group, 2000, NAG C Library Manual, Chapter 4, Mark 5, Oxford, England.

[11] Vollertsen, F., 1994, ''Mechanisms and Models for Laser Forming.'' *Laser Assisted Net Shape Engineering, Proceedings of the LANE'94*, Vol. 1, Meisenbach Bamberg, pp. 345–360.

[12] Struik, D. J., 1950, *Lectures on Classical Differential Geometry*, Addison-Wesley, Cambridge, MA.

[13] Dahlquist, G., and Bjorck, A., 1974, *Numerical Method*, Prentice-Hall, Englewood Cliffs, NJ.